

# Thermoelastic analysis of 3D generally anisotropic bodies by the boundary element method

Y. C. Shiah<sup>a</sup>  and C. L. Tan<sup>b</sup>

<sup>a</sup>Department of Aeronautics and Astronautics, National Cheng Kung University, Tainan, Taiwan, ROC;

<sup>b</sup>Department of Mechanical & Aerospace Engineering, Carleton University, Ottawa, Canada

## ABSTRACT

In the boundary element method (BEM) for stress analysis, it is well known that thermal loads give rise to an additional volume integral in the primary form of the boundary integral equation (BIE). This volume integral needs to be further transformed to surface ones in order to retain the characteristic of the BEM as a boundary solution technique. In this study of the BEM for 3D thermoelasticity in general anisotropy, the fundamental solutions are expressed as Fourier series with coefficients calculated using an explicit-form Green's function. In the exact volume-to-surface integral transformation associated with the term for the thermal effects in the BIE, a new kernel function is constructed. All formulations are implemented in an existing BEM code for 3D elastostatic analysis. Some numerical examples are presented to demonstrate the veracity of the formulations and the implementation, where the numerical results are compared with those obtained using the finite element method (FEM).

## ARTICLE HISTORY

Received 12 October 2015

Accepted 31 March 2016

## KEYWORDS

Three-dimensional anisotropic thermoelasticity; boundary element method; analytical volume-to-surface integral transformation

## 1. Introduction

In the direct formulation of the boundary integral equation (BIE) for the boundary element method (BEM), an additional volume integral arises when thermal loads are involved. If this integral is to be evaluated directly, it would require 'cell-discretisation' throughout the entire domain, destroying the notion of the BEM as a boundary solution technique. Over the years, several schemes have been proposed to overcome the need for domain discretisation. They include the dual reciprocity method (Nardini & Brebbia, 1982), the multiple reciprocity method (Nowak & Brebbia, 1989), the particular integral approach (Deb & Banerjee, 1990) and the exact transformation method (ETM) (Rizzo & Shippy, 1977). Among these schemes, the ETM is most appealing, not least because it restores the BIE to a true BIE without requiring analytical and/or numerical approximations, unlike the other schemes. For steady state, isotropic thermoelasticity, this volume integral

has been exactly transformed to boundary ones using the ETM for both 2D and 3D cases (Rizzo & Shippy, 1977). It has also been successfully achieved for 2D anisotropic thermoelasticity (Shiah & Tan, 1999) via a domain mapping technique (Shiah & Tan, 1997). However, the extension to the same end in BEM analysis for 3D generally anisotropic thermoelasticity poses a great challenge due to the mathematical complexity of the associated fundamental solutions.

The topic of numerical evaluation of the fundamental solution and its derivatives for 3D generally anisotropic elastic bodies has also remained a focus of numerous investigations for several decades (e.g. Pan & Yuan, 2000; Phan, Gray, & Kaplan, 2004; Sales & Gray, 1998; Tonon, Pan, & Amadei, 2001; Vogel & Rizzo, 1973; Wang & Denda, 2007; Wilson & Cruse, 1978). This is due to the fact that the Green's function presented in these cited works is not in closed, algebraic form. The fully explicit forms of the Green's function have only been developed in more recent years (see Lee, 2003, 2009; Shiah, Tan, & Lee, 2008; Tan, Shiah, & Lin, 2009; Ting & Lee, 1997). They allow their implementation into a BEM code with relatively greater ease, although they are still mathematically very elaborate. Indeed, the present lead authors further improved on the implementation as well as the computational efforts for the numerical evaluation of the fundamental solution and its derivatives in BEM by representing these quantities as a double Fourier series (Shiah, Tan, & Wang, 2012; Tan, Shiah, & Wang, 2013). Following this success, they also found that the double Fourier series representation of the Green's function and its derivatives can provide a very expedient means to facilitate the volume-to-surface integral transformation for the thermoelastic effects in the BIE in 3D general anisotropy (Shiah & Tan, 2014). This paper reports on the successful implementation of the ETM as described in that paper for the BEM thermoelastic analysis of 3D generally anisotropic solids. A brief review of the analytical basis will first be presented below, followed by some numerical examples.

## 2. BIE for anisotropic thermoelasticity

The analytical volume-to-surface integral transformation of the associated term in the BIE due to thermal loads for 3D general anisotropy has been described and presented by the present authors very recently (Shiah & Tan, 2014). Nevertheless, it is useful to provide a review of the key steps and the basic governing equations here. For a generally anisotropic elastic solid, the constitutive relationship between the stress  $\sigma_{ij}$  and the strain  $\varepsilon_{ij}$  with temperature change,  $\Theta$ , is governed by the well-known Duhamel–Neumann relation:

$$\sigma_{ij} = C_{ijkl}\varepsilon_{kl} - \gamma_{ij}\Theta, \quad (i, j, k, l = 1, 2, 3), \quad (1)$$

where  $\mathbf{C} = C_{ijkl}$  and  $\gamma_{ij}$  denote the elastic constants (stiffness coefficients) and thermal moduli of the material, respectively. The stiffness coefficients in  $\mathbf{C}$  used in the analysis here are arranged in the order according to:

$$\boldsymbol{\sigma} = (\sigma_{11}, \sigma_{22}, \sigma_{33}, \sigma_{23}, \sigma_{13}, \sigma_{12})^T, \quad \boldsymbol{\varepsilon} = (\varepsilon_{11}, \varepsilon_{22}, \varepsilon_{33}, 2\varepsilon_{23}, 2\varepsilon_{13}, 2\varepsilon_{12})^T. \quad (2)$$

For a generally anisotropic body, the thermal moduli in Equation (1) are given by:

$$\gamma_{ij} = C_{ijkl} \alpha_{kl}, \quad (3)$$

where  $\alpha_{kl}$  are the coefficients of thermal expansion. As in the usual manner to treat problems in steady-state, sequentially coupled thermoelasticity, the resulting elastic field is determined from the temperature distribution corresponding to the boundary conditions prescribed for heat conduction analysis. For this, the thermal field can be solved independently but must be first obtained before solving the elastostatic problem. Under the steady-state condition without heat source, the anisotropic heat conduction is governed in the Cartesian coordinate system by

$$K_{ij} \Theta_{,ij} = 0, \quad (i, j = 1, 2, 3), \quad (4)$$

where  $K_{ij}$  are the thermal conductivity coefficients. Equation (4) can be transformed to its canonical form of the Laplace equation by a simple coordinate transformation,

$$\hat{\mathbf{x}}^T = \mathbf{F} \mathbf{x}^T, \quad (5)$$

where  $\hat{\mathbf{x}}$  and  $\mathbf{x}$  represent the transformed and the original coordinates, respectively;  $\mathbf{F}$  denotes the transformation matrix with its coefficients defined by:

$$\mathbf{F} = \begin{pmatrix} \sqrt{\Delta}/K_{11} & 0 & 0 \\ -K_{12}/K_{11} & 1 & 0 \\ \lambda_1 & \lambda_2 & \lambda_3 \end{pmatrix}, \quad (6)$$

where,

$$\Delta = K_{11}K_{22} - K_{12}^2,$$

$$\lambda_1 = (K_{12}K_{23} - K_{13}K_{22})/\sqrt{\omega},$$

$$\lambda_2 = (K_{12}K_{13} - K_{23}K_{11})/\sqrt{\omega}, \quad (7)$$

$$\lambda_3 = \Delta/\sqrt{\omega}, \quad \omega = K_{11}K_{13}\Delta - K_{11}K_{12}K_{13}^2 + K_{11}K_{12}K_{13}K_{23} - K_{23}^2K_{11}^2.$$

Under the transformed coordinate system, the heat conduction is now governed by the standard Laplace equation,

$$\Theta_{\underline{.ii}} = 0, \quad (i = 1, 2, 3), \tag{8}$$

where the underscore is used to denote the new coordinate system. Once the temperature field in the body is determined via solving the BIE for the mapped domain, the solution for the corresponding elastic field of the solid body can then proceed.

As has been well established in the literature for the direct BEM formulation, the displacements  $u_i$  and the tractions  $t_i$  at the source point  $P$  and the field point  $Q$  on the surface  $S$  of an elastic body are related by the following integral equation,

$$\begin{aligned} C_{ij}(P)u_i(P) + \int_s u_i(Q)T_{ij}^*(P, Q)dS &= \int_s t_i(Q) U_{ij}^*(P, Q)dS \\ &+ \int_s \gamma_{ik}n_k(Q)\Theta(Q) U_{ij}^*(P, Q)dS - \int_\Omega \gamma_{ik}\Theta_{,k}(q) U_{ij}^*(P, q) d\Omega. \end{aligned} \tag{9}$$

It is clear that the last volume integral in Equation (9) needs to be transformed into surface ones for the equation to be truly a BIE. In the case of 2D general anisotropy, Shiah and Tan (1999) show that the volume integral can be analytically transformed to the boundary. The steps for the corresponding 3D case follow in the same general vein, although the analytical process becomes significantly more challenging due to the mathematically more complicated form of the fundamental solutions. A quick review of the fundamental solutions is thus in order before the integral transformation process is further discussed.

As derived by Ting and Lee (1997), the Green's function of displacements for 3D general anisotropy can be expressed in terms of the spherical coordinates  $(r, \theta, \phi)$  as

$$\mathbf{U}^*(\mathbf{x}) = \frac{1}{4\pi r} \frac{1}{|\boldsymbol{\kappa}|} \sum_{n=0}^4 q_n \hat{\Gamma}^{(n)}, \tag{10}$$

where  $r$  represents the radial distance between the source and the field point; and the quantities  $q_n$ ,  $\hat{\Gamma}^{(n)}$  and  $\boldsymbol{\kappa}$  are given by:

$$q_n = \begin{cases} \frac{-1}{2\beta_1\beta_2\beta_3} \left[ \text{Re} \left\{ \sum_{t=1}^3 \frac{p_t^n}{(p_t - \bar{p}_{t+1})(p_t - \bar{p}_{t+2})} \right\} - \delta_{n2} \right] & \text{for } n = 0, 1, 2, \\ \frac{1}{2\beta_1\beta_2\beta_3} \text{Re} \left\{ \sum_{t=1}^3 \frac{p_t^{n-2} \bar{p}_{t+1} \bar{p}_{t+2}}{(p_t - \bar{p}_{t+1})(p_t - \bar{p}_{t+2})} \right\} & \text{for } n = 3, 4, \end{cases} \tag{11a}$$

$$\hat{\Gamma}_{ij}^{(n)} = \tilde{\Gamma}_{(i+1)(j+1)(i+2)(j+2)}^{(n)} - \tilde{\Gamma}_{(i+1)(j+2)(i+2)(j+1)}^{(n)}, \quad (i, j = 1, 2, 3), \tag{11b}$$

$$\kappa_{ik} = C_{ijks} m_j m_s, \quad (11c)$$

$$\mathbf{m} = (-\sin \theta, \cos \theta, 0). \quad (11d)$$

In Equation (11a), the Stroh's eigenvalues,  $p_i$ , appear as three pairs of complex conjugates:

$$p_\nu = \alpha_\nu + i \beta_\nu, \quad \beta_\nu < 0, \quad (\nu = 1, 2, 3), \quad (12)$$

whose conjugates are denoted by  $\bar{p}_\nu$ . For more details regarding the variable definitions in Equation (11a) and (d), one can refer to Ting and Lee (1997). It is quite evident that carrying out spatial differentiations of Equation (10) to obtain the corresponding fundamental solution for tractions,  $T_{ij}^*$ , is cumbersome and less than straightforward. To simplify this, the present authors (Tan et al., 2013) rewrite the Green's function into a Fourier series form,

$$\mathbf{U}^* = \mathbf{H}(\theta, \phi)/4\pi r, \quad (13a)$$

$$H_{uv}(\theta, \phi) = \sum_{m=-a}^a \sum_{n=-a}^a \lambda_{uv}^{(m,n)} e^{i(m\theta+n\phi)}, \quad (u, v = 1, 2, 3), \quad (13b)$$

where  $a$  is an integer large enough to ensure convergence of the series;  $\lambda_{uv}^{(m,n)}$  are unknown coefficients determined, from the theory of Fourier series, by:

$$\lambda_{uv}^{(m,n)} = \frac{1}{4\pi^2} \int_{-\pi}^{\pi} \int_{-\pi}^{\pi} H_{uv}(\theta, \phi) e^{-i(m\theta+n\phi)} d\theta d\phi. \quad (14)$$

From previous studies,  $a = 16$  is adequate to ensure convergence of the series even for highly anisotropic material properties. By performing differentiations in the spherical coordinate system, the first-order derivatives of  $\mathbf{U}^*$ , denoted by  $\mathbf{U}^{*l}$ , may be expressed as:

$$U_{uv,l}^* = \frac{1}{4\pi r^2} \left\{ \begin{array}{l} \sum_{m=-a}^a \sum_{n=-a}^a \lambda_{uv}^{(m,n)} e^{i(m\theta+n\phi)} \begin{bmatrix} -\cos \theta (\sin \phi - i n \cos \phi) \\ -i m \sin \theta / \sin \phi \end{bmatrix} \quad \text{for } l = 1 \\ \sum_{m=-a}^a \sum_{n=-a}^a \lambda_{uv}^{(m,n)} e^{i(m\theta+n\phi)} \begin{bmatrix} -\sin \theta (\sin \phi - i n \cos \phi) \\ +i m \cos \theta / \sin \phi \end{bmatrix} \quad \text{for } l = 2 \\ \sum_{m=-a}^a \sum_{n=-a}^a \lambda_{uv}^{(m,n)} e^{i(m\theta+n\phi)} [-(\cos \phi + i n \sin \phi)] \quad \text{for } l = 3 \end{array} \right. \cdot \quad (15)$$

It is apparent that the computations in Equation (15) are fairly straightforward. The process of the volume-to-surface integral transformation will now be outlined.

### 3. BIE for anisotropic thermoelasticity

As explained previously, to restore the BEM as a truly boundary solution technique, the volume integral in Equation (9) needs to be transformed into a surface ones. For brevity, this integral is denoted by  $V_j$ , viz.

$$V_j = - \int_{\Omega} \gamma_{ik} \Theta_{,k} U_{ij}^* d\Omega, \quad (16)$$

where the notations of  $P$  and  $q$  in the integrand to, respectively, denote the source and the field point are omitted for conciseness. Similar to the transformation process for the 2D case (Shiah & Tan, 1999), the volume integral is, first, re-defined in the mapped domain using Equation (5) by:

$$V_j = - \int_{\underline{\Omega}} \Gamma_{ik} \underline{\Theta}_{,k}(q) \underline{U}_{ij}^*(P, q) d\underline{\Omega}, \quad (17)$$

where  $\Gamma_{ik}$  are the new thermal moduli, defined by (Shiah & Tan, 2004):

$$\Gamma_{ik} = K_{11} \sqrt{\frac{\omega}{\Delta^3}} \begin{pmatrix} \gamma_{11} & \gamma_{12} & \gamma_{13} \\ \gamma_{21} & \gamma_{22} & \gamma_{23} \\ \gamma_{31} & \gamma_{32} & \gamma_{33} \end{pmatrix} \begin{pmatrix} \sqrt{\Delta}/K_{11} & -K_{12}/K_{11} & \lambda_1 \\ 0 & 1 & \lambda_2 \\ 0 & 0 & \lambda_3 \end{pmatrix}. \quad (18)$$

The volume integral can be exactly transformed to the mapped surface  $\hat{S}$ , given by:

$$V_j = \int_{\hat{S}} \Gamma_{ik} \left[ \left( \Theta \underline{W}_{ijk,t}^* - \underline{W}_{ijk,t}^* \Theta_{,t} \right) \hat{n}_t - \Theta \underline{U}_{ij}^* \hat{n}_k \right] d\hat{S}, \quad (19)$$

where  $\underline{W}_{ijk}^*$  is a new kernel function introduced to satisfy:

$$\underline{W}_{ijk,tt}^* = \underline{U}_{ij,k}^*. \quad (20)$$

The analytical volume-to-surface integral transformation is not complete without explicitly determining the new function  $\underline{W}_{ijk}^*$ . In the mapped domain, the fundamental solution of displacements is expressed as:

$$\hat{U}^*(\hat{r}, \hat{\theta}, \hat{\phi}) = \frac{\hat{H}(\hat{\theta}, \hat{\phi})}{4\pi\hat{r}}. \quad (21)$$

In a similar manner, the Fourier series representation of  $\hat{H}(\hat{\theta}, \hat{\phi})$  is given by:

$$\hat{H}_{uv}(\theta, \hat{\phi}) = \sum_{m=-\alpha}^{\alpha} \sum_{n=-\alpha}^{\alpha} \hat{\lambda}_{uv}^{(m,n)} e^{i(m\hat{\theta}+n\hat{\phi})}, \quad (u, v = 1, 2, 3), \quad (22)$$

where the series coefficients are determined by:

$$\hat{\lambda}_{\underline{uv}}^{(m,n)} = \frac{1}{4\pi^2} \int_{-\pi}^{\pi} \int_{-\pi}^{\pi} \hat{H}_{\underline{uv}}(\hat{\theta}, \hat{\phi}) e^{-i(m\hat{\theta}+n\hat{\phi})} d\hat{\theta} d\hat{\phi}. \quad (23)$$

It is evident that  $\hat{H}_{\underline{uv}}(\hat{\theta}, \hat{\phi})$  can be determined using the  $\hat{\mathbf{U}}(\hat{x}_1, \hat{x}_2, \hat{x}_3)$ , defined in the Cartesian coordinate system for the mapped domain, as follows:

$$\hat{\mathbf{H}}(\hat{\theta}, \hat{\phi}) = 4\pi \hat{\mathbf{U}}^*(\sin \hat{\phi} \cos \hat{\theta}, \sin \hat{\phi} \sin \hat{\theta}, \cos \hat{\phi}). \quad (24)$$

By the coordinate transformation in Equation (5), Equation (24) can be rewritten as:

$$\hat{\mathbf{H}}(\hat{\theta}, \hat{\phi}) = 4\pi \mathbf{U}^*(x'_1, x'_2, x'_3), \quad (25)$$

where

$$\begin{aligned} x'_1 &= \frac{\sqrt{\Delta}}{K_{11}} \sin \hat{\phi} \cos \hat{\theta}, \\ x'_2 &= \frac{-K_{12}}{K_{11}} \sin \hat{\phi} \cos \hat{\theta} + \sin \hat{\phi} \sin \hat{\theta}, \\ x'_3 &= \lambda_1 \sin \hat{\phi} \cos \hat{\theta} + \lambda_2 \sin \hat{\phi} \sin \hat{\theta} + \lambda_3 \cos \hat{\phi}. \end{aligned} \quad (26)$$

Thus, Equation (23) is re-expressed as:

$$\hat{\lambda}_{\underline{uv}}^{(m,n)} = \frac{1}{4\pi^2} \int_{-\pi}^{\pi} \int_{-\pi}^{\pi} \frac{H_{\underline{uv}}(\theta', \phi')}{r'} e^{-i(m\theta'+n\phi')} d\theta' d\phi'. \quad (27)$$

In Equation (27),  $(r', \theta', \phi')$  are all intrinsic functions of  $(\hat{\theta}, \hat{\phi})$ , defined by:

$$r' = \sqrt{(x'_1)^2 + (x'_2)^2 + (x'_3)^2}, \quad \theta' = \tan^{-1} \left( \frac{x'_2}{x'_1} \right), \quad \phi' = \cos^{-1} \left( \frac{x'_3}{r'} \right). \quad (28)$$

As a result,  $\hat{\lambda}_{\underline{uv}}^{(m,n)}$  can be numerically computed using, for example, Gaussian quadrature, viz.

$$\hat{\lambda}_{\underline{uv}}^{(m,n)} = \frac{1}{4} \sum_{p=1}^k \sum_{q=1}^k w_p w_q \hat{f}_{\underline{uv}}^{(m,n)}(\pi \xi_p, \pi \xi_q), \quad (29)$$

where  $\hat{f}_{\underline{uv}}^{(m,n)}(\hat{\theta}, \hat{\phi})$  is the integrand in Equation (27), i.e.

$$\hat{f}_{\underline{uv}}^{(m,n)}(\hat{\theta}, \hat{\phi}) = \frac{H_{\underline{uv}}(\theta', \phi')}{r'} e^{-i(m\hat{\theta}+n\hat{\phi})}. \quad (30)$$

In Equation (30),  $H_{\underline{uv}}(\theta', \phi')$  is directly computed from Equation (13b). With all the coefficients,  $\hat{\lambda}_{\underline{uv}}^{(m,n)}$ , computed via the steps outlined above, the fundamental

displacements in the transformed coordinate system can be calculated using the Fourier series:

$$U_{\underline{uv}}^* = \frac{1}{4\pi\hat{r}} \sum_{m=-a}^a \sum_{n=-a}^a \hat{\lambda}_{\underline{uv}}^{(m,n)} e^{i(m\hat{\theta}+n\hat{\phi})}, \quad (u, v = 1, 2, 3) \quad (31)$$

Similar to Equation (15), the first-order derivatives of the fundamental displacements are given by:

$$U_{\underline{uv},l}^* = \frac{1}{4\pi\hat{r}^2} \begin{cases} \sum_{m=-a}^a \sum_{n=-a}^a \hat{\lambda}_{\underline{uv}}^{(m,n)} e^{i(m\hat{\theta}+n\hat{\phi})} \begin{bmatrix} -\cos\hat{\theta} (\sin\hat{\phi} - i n \cos\hat{\phi}) \\ -i m \sin\hat{\theta} / \sin\hat{\phi} \end{bmatrix} & \text{for } l = 1 \\ \sum_{m=-a}^a \sum_{n=-a}^a \hat{\lambda}_{\underline{uv}}^{(m,n)} e^{i(m\hat{\theta}+n\hat{\phi})} \begin{bmatrix} -\sin\hat{\theta} (\sin\hat{\phi} - i n \cos\hat{\phi}) \\ +i m \cos\hat{\theta} / \sin\hat{\phi} \end{bmatrix} & \text{for } l = 2 \\ \sum_{m=-a}^a \sum_{n=-a}^a \hat{\lambda}_{\underline{uv}}^{(m,n)} e^{i(m\hat{\theta}+n\hat{\phi})} [-(\cos\hat{\phi} + i n \sin\hat{\phi})] & \text{for } l = 3 \end{cases} \quad (32)$$

The remaining task to complete the volume integral transformation is the determination of  $W_{ijk}^*$ . In the spherical coordinate system for the mapped domain, Equation (20) can be expressed as:

$$\frac{\partial^2 W_{ijk}^*}{\partial \hat{r}^2} + \frac{2}{\hat{r}} \frac{\partial W_{ijk}^*}{\partial \hat{r}} + \frac{1}{\hat{r}^2} \frac{\partial^2 W_{ijk}^*}{\partial \hat{\phi}^2} + \frac{\cot\hat{\phi}}{\hat{r}^2} \frac{\partial W_{ijk}^*}{\partial \hat{\phi}} + \frac{1}{\hat{r}^2 \sin^2\hat{\phi}} \frac{\partial^2 W_{ijk}^*}{\partial \hat{\theta}^2} = \frac{\kappa_{ijk}(\hat{\theta}, \hat{\phi})}{\hat{r}^2}, \quad (33)$$

where,

$$\kappa_{ijk}(\hat{\theta}, \hat{\phi}) = \frac{1}{4\pi} \begin{cases} \sum_{m=-a}^a \sum_{n=-a}^a \hat{\lambda}_{ij}^{(m,n)} e^{i(m\hat{\theta}+n\hat{\phi})} \begin{bmatrix} -\cos\hat{\theta} (\sin\hat{\phi} - i n \cos\hat{\phi}) \\ -i m \sin\hat{\theta} / \sin\hat{\phi} \end{bmatrix} & \text{for } k = 1 \\ \sum_{m=-a}^a \sum_{n=-a}^a \hat{\lambda}_{ij}^{(m,n)} e^{i(m\hat{\theta}+n\hat{\phi})} \begin{bmatrix} -\sin\hat{\theta} (\sin\hat{\phi} - i n \cos\hat{\phi}) \\ +i m \cos\hat{\theta} / \sin\hat{\phi} \end{bmatrix} & \text{for } k = 2 \\ \sum_{m=-a}^a \sum_{n=-a}^a \hat{\lambda}_{ij}^{(m,n)} e^{i(m\hat{\theta}+n\hat{\phi})} [-(\cos\hat{\phi} + i n \sin\hat{\phi})] & \text{for } k = 3 \end{cases} \quad (34)$$

To satisfy Equation (33),  $W_{ijk}^*$  must be dependent on the spherical angles only and thus, it is written simply as  $\underline{W}_{ijk}^*(\hat{\theta}, \hat{\phi})$ . As a result, Equation (33) is simplified to:

$$\sin^2\hat{\phi} \frac{\partial^2 \underline{W}_{ijk}^*(\hat{\theta}, \hat{\phi})}{\partial \hat{\phi}^2} + \frac{\sin 2\hat{\phi}}{2} \frac{\partial \underline{W}_{ijk}^*(\hat{\theta}, \hat{\phi})}{\partial \hat{\phi}} + \frac{\partial^2 \underline{W}_{ijk}^*(\hat{\theta}, \hat{\phi})}{\partial \hat{\theta}^2} = \kappa_{ijk}(\hat{\theta}, \hat{\phi}) \sin^2\hat{\phi}. \quad (35)$$

By taking advantage of the periodic nature of the spherical angles,  $\underline{W}_{ijk}^*(\hat{\theta}, \hat{\phi})$  can be expressed as a Fourier series as well; thus,

$$W_{ijk}^*(\hat{\theta}, \hat{\phi}) = \sum_{m=-a}^a \sum_{n=-a}^a \tilde{C}_{ijk}^{(m,n)} e^{i(m\hat{\theta}+n\hat{\phi})}, \quad (36)$$

where  $\tilde{C}_{ijk}^{(m,n)}$  are unknown coefficients to be determined. Substituting Equation (36) directly into Equation (35) yields:

$$\frac{-1}{2} \sum_{m=-a}^a \sum_{n=-a}^a \tilde{C}_{ijk}^{(m,n)} (n^2 + 2m^2 - n^2 \cos 2\hat{\phi} - in \sin 2\hat{\phi}) e^{i(m\hat{\theta}+n\hat{\phi})} = \kappa_{ijk}(\hat{\theta}, \hat{\phi}) \sin^2 \hat{\phi}. \quad (37)$$

For determining the unknown coefficients, both sides of Equation (37) are integrated as follows:

$$\begin{aligned} \frac{-1}{2\pi^2} \int_{-\pi}^{\pi} \int_{-\pi}^{\pi} \sum_{m=-a}^a \sum_{n=-a}^a \tilde{C}_{ijk}^{(m,n)} (n^2 + 2m^2 - n^2 \cos 2\hat{\phi} - in \sin 2\hat{\phi}) e^{i(m\hat{\theta}+n\hat{\phi})} e^{-i(p\hat{\theta}+q\hat{\phi})} d\hat{\theta} d\hat{\phi} \\ = \frac{1}{\pi^2} \int_{-\pi}^{\pi} \int_{-\pi}^{\pi} \kappa_{ijk}(\hat{\theta}, \hat{\phi}) \sin^2 \hat{\phi} e^{-i(p\hat{\theta}+q\hat{\phi})} d\hat{\theta} d\hat{\phi} \end{aligned} \quad (39)$$

As a result of performing the above integrations for  $p, q$  ranging from  $-a$  to  $+a$ , one obtains:

$$\tilde{\mathbf{C}}_{ijk} = \mathbf{M}^{-1} \mathbf{Y}_{ijk}, \quad (38)$$

where  $\tilde{\mathbf{C}}_{ijk}$  is the matrix with each set of  $\tilde{C}_{ijk}^{(m,n)}$  numbered in the sequential order,  $\mathbf{Y}_{ijk}$  represents the integration values on the right hand side of Equation (38), and  $\mathbf{M}$  is the banded matrix obtained from the integration of the left hand side of Equation (38). More details regarding the determination of  $\tilde{C}_{ijk}^{(m,n)}$  can be found in Shiah and Tan (2014) and thus, no further discussion is made here. With all coefficients determined by Equation (39),  $W_{ijk}^*(\hat{\theta}, \hat{\phi})$  is computed using Equation (36) and its first-order derivatives are given by:

$$W_{ijk,t}^*(\hat{r}, \hat{\theta}, \hat{\phi}) = \frac{1}{\hat{r}} \begin{cases} \sum_{m=-a}^a \sum_{n=-a}^a \tilde{C}_{ijk}^{(m,n)} e^{i(m\hat{\theta}+n\hat{\phi})} (in \cos \hat{\theta} \cos \hat{\phi} - im \sin \hat{\theta} / \sin \hat{\phi}) & (\text{for } t = 1) \\ \sum_{m=-a}^a \sum_{n=-a}^a \tilde{C}_{ijk}^{(m,n)} e^{i(m\hat{\theta}+n\hat{\phi})} (in \sin \hat{\theta} \cos \hat{\phi} + im \cos \hat{\theta} / \sin \hat{\phi}) & (\text{for } t = 2) \\ \sum_{m=-a}^a \sum_{n=-a}^a \tilde{C}_{ijk}^{(m,n)} e^{i(m\hat{\theta}+n\hat{\phi})} (-in \sin \hat{\phi}) & (\text{for } t = 3) \end{cases}. \quad (40)$$

Since the formulations of  $W_{ijk}^*(\hat{\theta}, \hat{\phi})$  and  $W_{ijk,t}^*(\hat{r}, \hat{\theta}, \hat{\phi})$  have been explicitly defined, the transformed surface integral, Equation (19), can be numerically evaluated in a straightforward manner.

#### 4. Numerical examples

All the formulations described above have been implemented in an existing BEM code based on the quadratic isoparametric element. Three examples are presented here to illustrate its successful implementation. The material properties of alumina  $\text{Al}_2\text{O}_3$  crystal (Shiah & Tan, 2004) were chosen for the thermoelastic analyses of these problems. It has the following stiffness constants:

$$C_{11} = 465 \text{ GPa}, C_{33} = 563 \text{ GPa}, C_{44} = 233 \text{ GPa}, \quad (41)$$

$$C_{12} = 124 \text{ GPa}, C_{13} = 117 \text{ GPa}, C_{14} = 101 \text{ GPa},$$

Also, the following thermal properties were used in the analysis:

$$K_{11}^* = 18 \text{ (W/m } ^\circ\text{C)}, \quad K_{22}^* = 10 \text{ (W/m } ^\circ\text{C)}, \quad K_{33}^* = 25 \text{ (W/m } ^\circ\text{C)}, \quad (42)$$

$$\alpha_{11}^* = 8.1 \times 10^{-6} \text{ (1/} ^\circ\text{C)}, \quad \alpha_{22}^* = 5.4 \times 10^{-6} \text{ (1/} ^\circ\text{C)}, \quad \alpha_{33}^* = 9.2 \times 10^{-6} \text{ (1/} ^\circ\text{C)}.$$

To treat the problem as a generally anisotropic case, the principal material axes were rotated with respect to the  $x_3$ -,  $x_1$ - and  $x_2$ -axis by  $60^\circ$ ,  $45^\circ$ ,  $30^\circ$  counterclockwise, respectively, in succession. This results in the following material constants in the global Cartesian coordinate system:

$$\mathbf{C} = \begin{pmatrix} 620.616 & 53.593 & 87.202 & 39.992 & -18.414 & -58.115 \\ 53.593 & 513.175 & 140.699 & 73.644 & 6.364 & 65.699 \\ 87.202 & 140.699 & 512.227 & -106.569 & 55.535 & 1.423 \\ 39.992 & 73.644 & -106.569 & 214.376 & 8.301 & 39.574 \\ -18.414 & 6.364 & 55.535 & 8.301 & 202.085 & 45.390 \\ -58.115 & 65.699 & 1.423 & 39.574 & 45.390 & 143.531 \end{pmatrix} \text{ (GPa)}, \quad (43a)$$

$$\mathbf{K} = \begin{pmatrix} 19.262 & 2.425 & 6.809 \\ 2.425 & 17.113 & -1.456 \\ 6.809 & -1.456 & 16.625 \end{pmatrix} \text{ (W/m} ^\circ\text{C)} \quad (43b)$$

$$\boldsymbol{\alpha} = \begin{pmatrix} 7.75731 & 0.69343 & 1.69477 \\ 0.69343 & 7.78019 & -0.58957 \\ 1.69477 & -0.58957 & 7.16250 \end{pmatrix} \times 10^{-6} \text{ (1/} ^\circ\text{C)} \quad (43c)$$

Figure 1(a) shows the first example considered. It is a thick plate with its two opposite ends fully constrained. All surfaces except the constrained ends are traction-free. For the thermal boundary conditions, the end at  $x_2 = L/2$  is prescribed

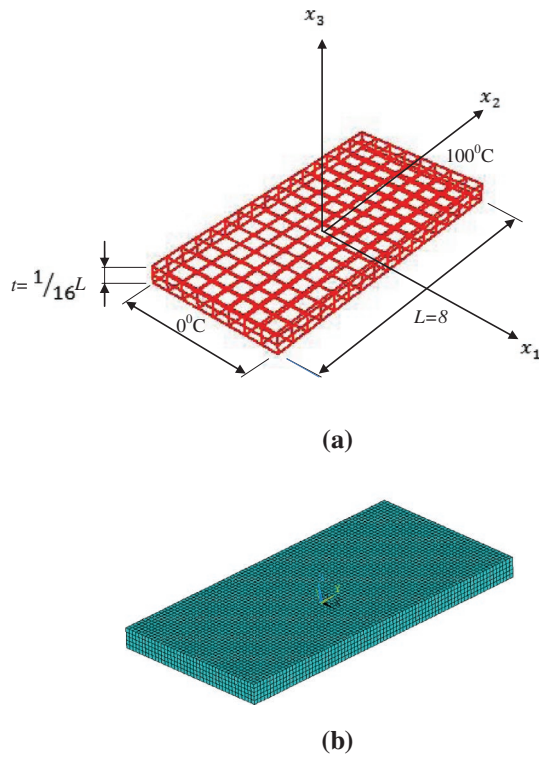


**Figure 1.** Modelling of a thick rectangular plate by (a) BEM and (b) ANSYS FEM.

with  $0\text{ }^{\circ}\text{C}$  and the opposite end is  $100\text{ }^{\circ}\text{C}$ ; all the other surfaces are thermally insulated. Also shown in Figure 1(a) is the mesh employed for the BEM analysis; it has 352 elements. For the purpose of verification of the BEM results, the problem is also analysed using ANSYS FEM with 83,780 SOLIDS226 elements (Figure 1(b)). The resultant displacements ( $u_0 = \sqrt{u_1^2 + u_2^2 + u_3^2}$ ) at the nodes along the centrelines on the top and bottom surfaces are calculated and normalised by the quantity  $L \alpha_{11} \Delta\Theta$ , where  $\Delta\Theta = 100\text{ }^{\circ}\text{C}$  is the temperature difference between the constrained ends. The variations of the calculated resultant displacements are shown in Figure 2 for both the BEM and FEM results. The von Mises equivalent stress at these locations is also calculated and plotted in Figure 3. As can be seen from these plots, the agreement between the BEM and FEM results is very good indeed.

For the second example, consider a thick-walled tube with one end (bottom) closed with an integrated end plate as shown in Figure 4(a); the dimensions are as indicated. The outside wall and the bottom are fully constrained and all other surfaces are traction-free. For the thermal boundary conditions, the exterior constrained surfaces are prescribed with  $0\text{ }^{\circ}\text{C}$ , and the inner surfaces, including the bottom and the inner cylinder wall, are prescribed  $100\text{ }^{\circ}\text{C}$ ; the top end is thermally insulated. Figure 4(a) and (b) shows the mesh discretisations of the BEM

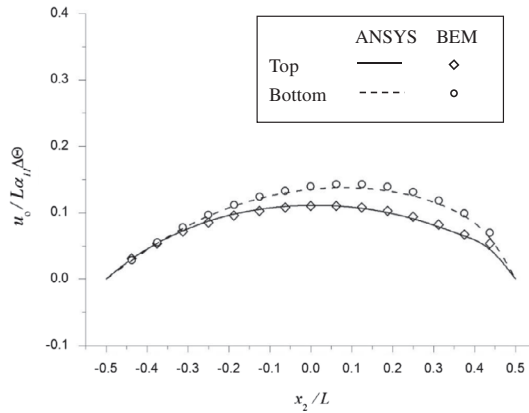


**Figure 2.** Resultant displacement along the centreline ( $x_1 = 0$ ) of the thick plate.

and ANSYS analyses, where 608 and 83,780 SOLIDS226 elements were used, respectively. The resultant displacements at the nodes around the periphery of the inner surface on the  $x_1-x_2$  plane are calculated and normalised by the same factor as in the previous case. The normalised resultant displacements at these nodes are plotted in Figure 5. The hoop stress  $\sigma_{\theta\theta}$  and the axial stress  $\sigma_{33}$  at the nodes on the inner and outer surfaces in the  $x_1-x_2$  plane are also plotted in Figures 6 and 7, respectively. As can be seen from the comparisons in these plots, very good agreement is again obtained between the results of the BEM and ANSYS analyses.

The last example treats a thick-walled hollow sphere with the inner radius,  $r_i = 1$  unit and outer radius,  $r_o = 2$  units. The outside surface is fully constrained and the inner is free to displace in all directions. For the thermal boundary condition, the inner and outer surfaces are prescribed with  $100\text{ }^\circ\text{C}$  and  $0\text{ }^\circ\text{C}$  ( $\Delta\Theta = 100\text{ }^\circ\text{C}$ ), respectively. Figure 8(a) and (b) displays the meshes used in the BEM and ANSYS analyses, where 680 elements and 61,440 SOLIDS226

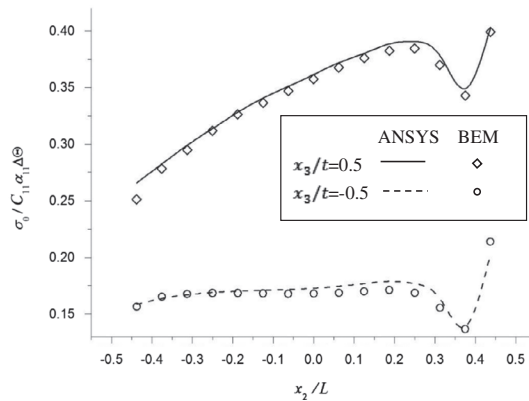


**Figure 3.** Equivalent stress along the centreline ( $x_1 = 0$ ) of the thick plate.

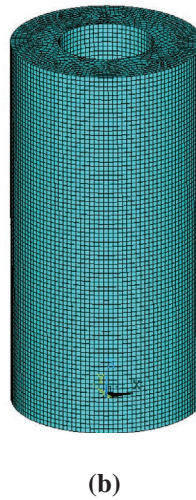
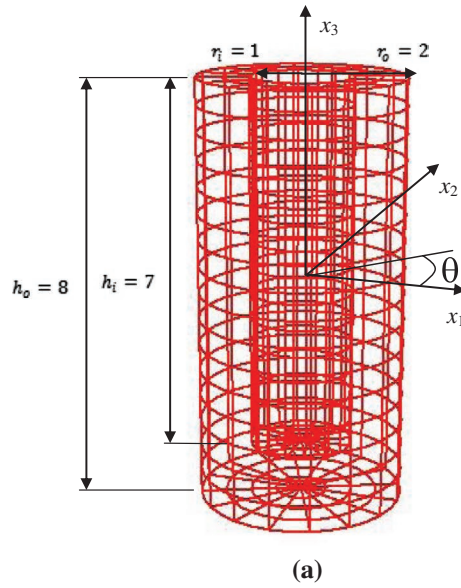


**Figure 4.** Modelling of a thick-walled tube under thermal gradient: (a) BEM mesh, (b) ANSYS FEM mesh.

elements are, respectively, employed. Similar to the analyses in the previous example, the resultant displacement at the nodes around the equators of the inner and outer surfaces is calculated, and their normalised values are plotted in Figure 9. The normalised  $\sigma_{\theta\theta}$  and  $\sigma_{33}$  are also plotted in Figures 10 and 11, respectively. Excellent agreement between the results obtained from the BEM and FEM analyses are again achieved.

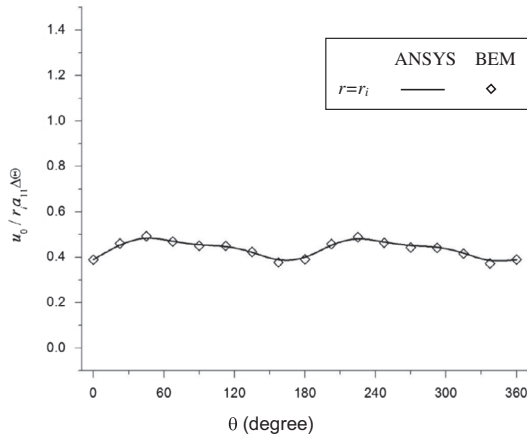


**Figure 5.** Variation of the normalised resultant displacement around the inner surface of the tube at the  $x_3 = 0$  plane.

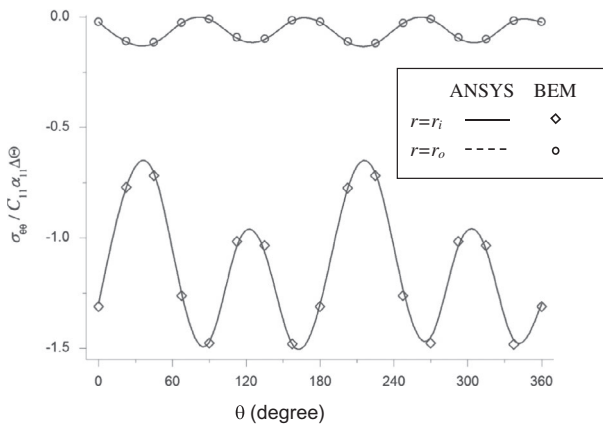


**Figure 6.** Variations of the normalised hoop stresses at the inner and outer surfaces of the tube at the  $x_3 = 0$  plane.

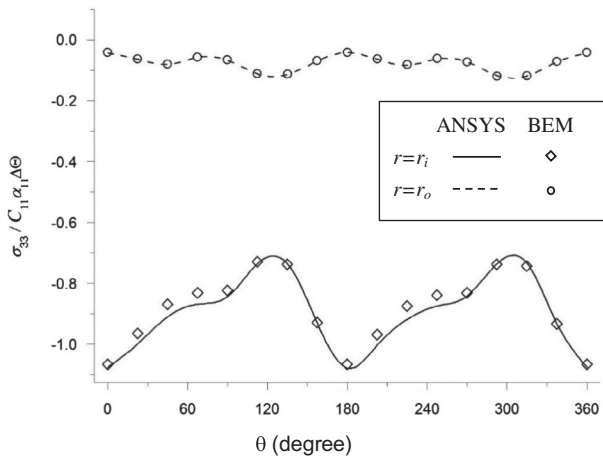
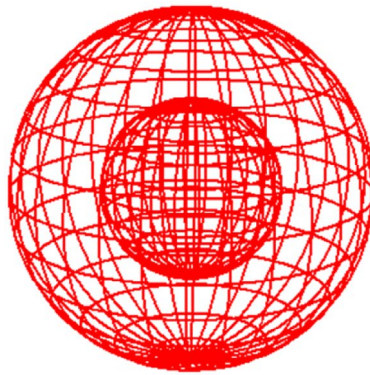
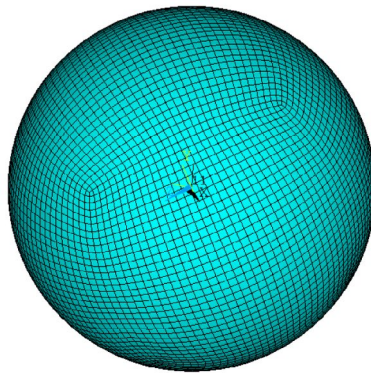


**Figure 7.** Variations of the normalised axial stresses at the inner and outer surfaces of the tube on the  $x_3 = 0$  plane.



(a)



(b)

**Figure 8.** Modelling of the thick-walled hollow sphere by (a) BEM, (b) ANSYS.

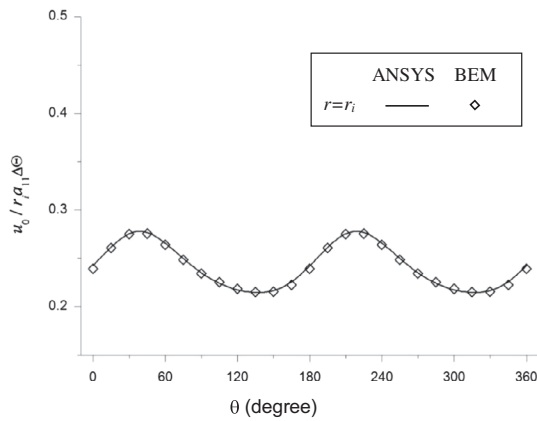


**Figure 9.** Variation of the normalised resultant displacement around the equator of the inner surface of the sphere.

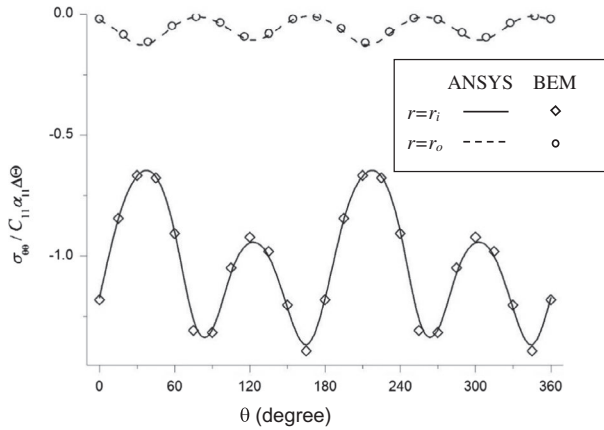


**Figure 10.** Variations of the normalised hoop stresses along the equators of the inner and outer surfaces of the hollow sphere.

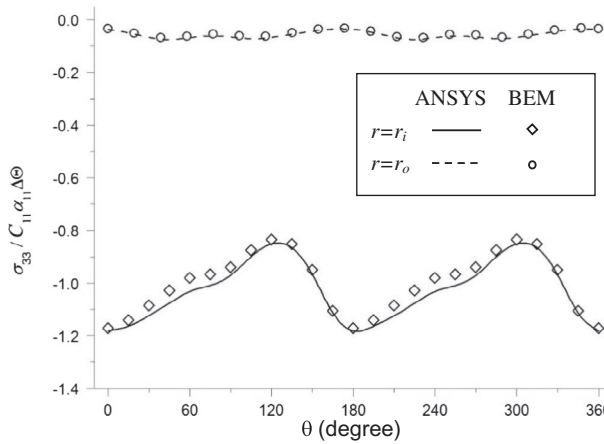


**Figure 11.** Variation of the normalised stress  $\sigma_{33}$  along the equators of the inner and outer surfaces of the hollow sphere.

### 5. Conclusions

The ETM that transforms analytically the additional volume integral associated with thermal effects in the BIE to surface integrals has been achieved and implemented for BEM in 3D general anisotropic thermoelasticity. This has never been successfully undertaken in the literature because of the mathematical complexity of the Green’s function. The approach followed the same key steps developed by the lead authors for the 2D case previously, together with the use of the double Fourier representation of the 3D Green’s function. The transformed surface integrals have been successfully implemented into an existing BEM code. This has been illustrated by some examples in which numerical results have been compared with those obtained using ANSYS FEM analysis using very refined meshes.

Excellent agreement between the results obtained using both numerical schemes have been obtained.

### Acknowledgements

The first author gratefully acknowledges the financial support from the Ministry of Science and Technology of Taiwan (No. 102-2221-E-006-290-MY3).

### Disclosure statement

No potential conflict of interest was reported by the authors.

### Funding

This work was supported by the Ministry of Science and Technology of Taiwan [No. 102-2221-E-006-290-MY3].

### ORCID

Y. C. Shiah  <http://orcid.org/0000-0002-6016-1426>

### References

- Deb, A., & Banerjee, P. K. (1990). BEM for general anisotropic 2D elasticity using particular integrals. *Communications in Applied Numerical Methods*, 6, 111–119.
- Lee, V. G. (2003). Explicit expression of derivatives of elastic Green's functions for general anisotropic materials. *Mechanics Research Communications*, 30, 241–249.
- Lee, V. G. (2009). Derivatives of the three-dimensional Green's function for anisotropic materials. *International Journal of Solids and Structures*, 46, 1471–1479.
- Nardini, D., & Brebbia, C. A. (1982). *A new approach to free vibration analysis using boundary elements*, *Boundary Element Methods in Engineering*. Southampton: Computational Mechanics Publications.
- Nowak, A. J., & Brebbia, C. A. (1989). The multiple-reciprocity method. A new approach for transforming BEM domain integrals to the boundary. *Engineering Analysis with Boundary Elements*, 6, 164–167.
- Pan, E., & Yuan, F. G. (2000). Boundary element analysis of three dimensional cracks in anisotropic solids. *International Journal for Numerical Methods in Engineering*, 48, 211–237.
- Phan, A.-V., Gray, L. J., & Kaplan, T. (2004). On the residue calculus evaluation of the 3-D anisotropic elastic green's function. *Communications in Numerical Methods in Engineering*, 20, 335–341.
- Rizzo, F. J., & Shippy, D. J. (1977). An advanced boundary integral equation method for three-dimensional thermoelasticity. *International Journal for Numerical Methods in Engineering*, 11, 1753–1768.
- Sales, M. A., & Gray, L. J. (1998). Evaluation of the anisotropic Green's function and its derivatives. *Computers and Structures*, 69, 247–254.
- Shiah, Y. C., & Tan, C. L. (1997). BEM treatment of two-dimensional anisotropic field problems by direct domain mapping. *Engineering Analysis with Boundary Elements*, 20, 347–351.

- Shiah, Y. C., & Tan, C. L. (1999). Exact boundary integral transformation of the thermoelastic domain integral in BEM for general 2D anisotropic elasticity. *Computational Mechanics*, 23, 87–96.
- Shiah, Y. C., & Tan, C. L. (2004). BEM treatment of three-dimensional anisotropic field problems by direct domain mapping. *Engineering Analysis with Boundary Elements*, 28, 43–52.
- Shiah, Y. C., & Tan, C. L. (2014). The boundary integral equation for 3D general anisotropic thermoelasticity. *CMES Computer Modeling in Engineering Sciences*, 102, 425–447.
- Shiah, Y. C., Tan, C. L., & Lee, V. G. (2008). Evaluation of explicit-form fundamental solutions for displacements and stresses in 3D anisotropic elastic solids. *CMES Computer Modeling in Engineering Sciences*, 34, 205–226.
- Shiah, Y. C., Tan, C. L., & Wang, C. Y. (2012). Efficient computation of the Green's function and its derivatives for three-dimensional anisotropic elasticity in BEM analysis. *Engineering Analysis with Boundary Elements*, 36, 1746–1755.
- Tan, C. L., Shiah, Y. C., & Lin, C. W. (2009). Stress analysis of 3D generally anisotropic elastic solids using the boundary element method. *CMES Computer Modeling in Engineering Sciences*, 41, 195–214.
- Tan, C. L., Shiah, Y. C., & Wang, C. Y. (2013). Boundary element elastic stress analysis of 3D generally anisotropic solids using fundamental solutions based on Fourier series. *International Journal of Solids and Structures*, 50, 2701–2711.
- Ting, T. C. T., & Lee, V. G. (1997). The three-dimensional elastostatic Green's function for general anisotropic linear elastic solids. *The Quarterly Journal of Mechanics and Applied Mathematics*, 50, 407–426.
- Tonon, F., Pan, E., & Amadei, B. (2001). Green's functions and boundary element method formulation for 3D anisotropic media. *Computers and Structures*, 79, 469–482.
- Vogel, S. M., & Rizzo, F. J. (1973). An integral equation formulation of three dimensional anisotropic elastostatic boundary value problems. *Journal of Elasticity*, 3, 203–216.
- Wang, C.-Y., & Denda, M. (2007). 3D BEM for general anisotropic elasticity. *International Journal of Solids and Structures*, 44, 7073–7091.
- Wilson, R. B., & Cruse, T. A. (1978). Efficient implementation of anisotropic three-dimensional boundary integral equation stress analysis. *International Journal for Numerical Methods in Engineering*, 12, 1383–1397.